

**[DEVELOPING SHELF STABLE FORMULATIONS TO IMPROVE THE
INDUSTRIAL UTILIZATION OF LIGNIN IN AUTOMOTIVE TIRES]**

A Dissertation

Presented to

The Academic Faculty

by

Clara Templin

In Partial Fulfillment

Of the Requirements for the Degree

Bachelor of Science in the

School of Materials Science and Engineering

Georgia Institute of Technology

May 2025

[DEVELOPING SHELF STABLE FORMULATIONS TO IMPROVE THE INDUSTRIAL UTILIZATION OF LIGNIN IN AUTOMOTIVE TIRES]

Approved by:

Dr. Scott Danielsen, Advisor

School of Materials Science and Engineering

Georgia Institute of Technology


Signed by:

2F2BD0A3657F4F6...

Dr. Meisha Shofner

School of Materials Science and Engineering

Georgia Institute of Technology

DocuSigned by:

B1AA124FA253489...

Date Approved: [April 23, 2025]

TABLE OF CONTENTS

<i>TABLE OF CONTENTS</i>	2
<i>ABSTRACT</i>	3
<i>INTRODUCTION</i>	4
<i>LITERATURE REVIEW</i>	6
<i>MATERIALS AND METHODS</i>	14
<i>A. Sample Formulation</i>	14
<i>B. Dynamic Light Scattering Testing</i>	15
<i>RESULTS AND DISCUSSION</i>	16
<i>A. Autocorrelation Function</i>	16
<i>B. CORENN Intensity</i>	21
<i>C. Impact of Additives on Hydrodynamic Radius</i>	25
<i>FUTURE WORK</i>	28
<i>REFERENCES</i>	29

ABSTRACT

The disposal of used automotive tires presents a significant environmental challenge, compounded by the tire industry's reliance on non-renewable petrochemical materials such as carbon black. This research explores the development of shelf-stable natural rubber-lignin formulations as sustainable alternatives for tire manufacturing. Specifically, the study investigates how varying pH and ionic conditions affect the stability of natural rubber (NR) latex mixed with plant-derived lignin. Dynamic Light Scattering (DLS) analysis revealed that mildly acidic conditions improved the colloidal stability of the rubber-lignin matrix, slightly reducing particle size distribution and polydispersity, whereas basic and ionic conditions generally destabilized the formulation. These findings contribute toward the industrial viability of lignin-based, environmentally friendly tire materials and inform future work focused on additive optimization and 3D printing compatibility of uncured rubber systems.

INTRODUCTION

In 2021, the transportation sector consumed a quarter of global energy, generating 7.7 Gt of CO₂ and accounting for 40% of global greenhouse gas emissions for that year. Ground vehicles specifically contributed 5.9 Gt of that 7.7 Gt total or approximately 29% of global greenhouse gas emissions for that year [1]. Ground vehicles also generate a substantial amount of solid waste, a large portion of which is through the disposal of used tires. To further quantify the problem, an estimated 1.5 billion used whole tires are discarded each year with the majority ending up in landfills and other waste stockpiles [2]. The number of tires discarded each year is also expected to increase due to population growth and economic development in lower-income countries which would increase demand for both personal and commercial ground vehicles [3].

While there have been steps towards reducing the quantity of end-of-life tires worldwide, an overwhelming majority of waste tires still end up in landfills. Fields such as civil engineering and geoengineering have attempted to utilize waste tires in various construction materials/applications, but these attempts have had limited success [2, 4, 5]. In landfills, tires endanger public health via fire risks, house disease-carrying pests, and leach harmful chemicals and metals into the environment [6, 7]. Recycling is not regarded as an optimal solution either. Recycling used tires is difficult due to their complex construction; tires consist of multiple layers of multi-component materials that require large amounts of time and energy to successfully separate. Even when separated, materials like recycled rubber often exhibit inferior mechanical properties when compared to virgin rubber due to remnant impurities and chemical incompatibility between batches. Material extraction processes such as pyrolysis allow the extraction of pyrolysis oil, carbon black, and pyrolytic gas from waste tires. Given that carbon black is a nonrenewable petrochemical byproduct, extracting it from used tires is beneficial in

reducing energy and material consumption and allows the reclaimed carbon black to be incorporated back into new tires [6].

Petrochemical-derived materials are crucial in the fabrication of tires today with carbon black being the most significant, providing tires with key features such as their durability, structure, color, and stability [6]. These non-renewable petrochemical materials contribute significantly to the overall emissions and environmental impacts of the tires [8]. In the wider field of sustainable tire materials, there has been increased interest in materials derived from renewable resources and various types of biowaste. For example, different sources of natural rubber (hevea, dandelion, guayule, etc.), bio-based polyester and thermoplastic elastomers, and agricultural-based silica and graphene are increasingly subjects of interest [9].

This research fits into the broader context of renewable tire materials that have a lower environmental impact when compared to traditional tires. In partnership with a tire material start-up, we are interested in making shelf-stable tire formulations consisting of natural rubber, silica, and plant-based lignin. Current formulations often experience phase separation when left undisturbed, preventing effective storage of un-vulcanized rubber mixtures. Once vulcanized, these tires are used with large vehicles like trucks and buses and exhibit increased durability and fuel efficiency when compared to traditional petroleum-based tires. The objective of the conducted research is to test the impact of varying pH and ionic conditions on the stability of the starting natural rubber latex and lignin formulation and determine next steps for developing the optimal shelf-stable formulation.

LITERATURE REVIEW

To combat growing used tire waste and keep more waste tires out of landfills, fields such as construction, civil engineering, and geoen지니어ing have sought ways to utilize waste tires as a valuable material in their own right. To utilize them, waste tires are typically shredded before applications in building insulation, cement additives, “light filling in the construction of tunnels and underground passages” [4], road pavement, playground flooring/ground cover, concrete fill, soil stabilization, and reduced weight embankments to list a few [2, 4]. Tire materials are ideal for such applications due to material properties such as low density, good thermal insulation, drainage ability, long-term durability, “high compressibility, and low earth pressure” [5]. Despite these apparent advantages, the actual percentage of waste tires used in geotechnical applications is quite low. In the US, only 7.8% of waste tires were used in geotechnical applications in 2011, and the EU had a similarly low quantity of 7.4% in 2010 [5].

Because tires are non-biodegradable, they sit in the environment and landfills for decades, posing fire risks, serving as breeding grounds for disease carrying pests like mosquitoes and rodents, and leaching harmful chemicals [6, 10]. Waste tire stockpiles pose fire risks, particularly during dry seasons, due to the large amount of energy stored in the tire materials and empty space within the tires that provide oxygen to the fires [6, 11]. The burning of waste tires, both through accidental fires and intentional incineration, releases small particulates and toxic, acidic fumes into the environment [12, 13]. Water is not seen as an ideal method to extinguish such fires because it provides a path for other harmful pollutants to enter the environment, resulting in fires burning for long periods of time as was the case at Tyre King Recycling in Canada where a fire there lasted for 17 days before being extinguished [6]. Empty space within the tires also provides breeding grounds for disease-carrying pests such as rodents and snakes, and the collection of

water in empty tires similarly allows mosquito populations to grow and spread diseases like dengue, Zika, chikungunya, and West Nile [6, 10]. Even when not on fire, whole discarded tires, shredded waste tires used in construction/geotechnical projects, and microplastics released from the tires via road friction negatively impact the environment, leaching harmful chemicals and metals into terrestrial and aquatic ecosystems and harming the organisms living there [7].

Recycling is also not regarded as a good long-term method to deal with waste tires. Tire construction is complex with layering of multi-component materials that contain blends of natural and synthetic rubbers, carbon black, silica, metals like steel, textiles, vulcanizing agents, and other additives. The relative proportion of these materials also varies depending on manufacturer and intended vehicle/use, making the separation of material components and the recycling of end-of-life tires both time and energy intensive. In the case of rubber, great care must be taken to separate non-rubber materials as impurities significantly impact the structure of the recycled rubber, and even with these precautions, the resulting recycled rubber can still exhibit inferior mechanical properties when compared to virgin rubber due to chemical incompatibility between batches [6, 11]. Pyrolysis is another key material extraction technique used on waste tires that involves the thermal decomposition of the rubber in an oxygen-free environment [11]. The high heat environment allows the extraction of valuable resources such as pyrolysis oil, carbon black, pyrolytic gas, and steel cord [6, 11]. The pyrolysis oil and gas can be used directly to generate heat and electricity or refined further into other industrially useful chemicals. The carbon black and steel cord can be used again in new tires. Despite the advantage of material recovery via pyrolysis, the process is energy intensive and expensive [11].

Key material components like carbon black (crucial in ensuring the stability and longevity of tires) and synthetic rubbers including polybutadiene and styrene-butadiene rubber (help form the

rubber matrix) carry their own environmental implications [6]. Carbon black and both synthetic rubbers listed are non-renewable byproducts of the petrochemical industry. While there has been progress in the use of recycled carbon black (from pyrolysis) and increased research into carbon black made from non-traditional sources including “methane, carbon dioxide, vegetable oil, and scrap tire pyrolysis oil,” the majority of carbon black used in automobile tires is still from petrochemical sources [9].

The utilization of carbon black contributes a significant portion of the life-cycle greenhouse gas emissions for rubber-base composites. According to a 2017 study examining the life-cycle carbon emissions of e-bike tires produced at a Taiwanese factory, raw materials contribute the largest proportion of life-cycle carbon emissions at 58.06% with production inside the plant contributing the second most at 28.59% [8]. At the raw material stage, the study found carbon black to be the largest contributor to carbon emissions at 23.90% of the 4.53 kg CO₂ in total emissions for the specific tire formulation used [8]. When the carbon black was replaced with graphene, properties of the resulting rubber improved, and carbon emissions were reduced by between 24.81% and 98.81% depending on the weight percentage of carbon black replaced with graphene [8]. Considering carbon black makes up anywhere between 21% and 28% of tires, its replacement with more environmentally sustainable materials could be a major source of emission reductions [6, 11].

There has been increased academic and industrial interest in renewable tire materials that could replace nonrenewables such as carbon black. Tire materials can be sorted into five main groups: rubber which forms the main structure of the tire, metal inserts like steel that reinforce the structure of the tire, tire cords that run throughout the rubber matrix and provide a frame for the matrix to adhere, vulcanizing agents which facilitate key chemical reactions, and other additives

that impart new/improved chemical and mechanical properties [6, 11]. Of these groups, research into alternative and renewable materials primarily centers on rubbers, tire cords, and tire additives including filler materials, synthetic oils, and chemical promoters and activators [9].

Rubber can further be divided into natural and synthetic rubbers. Natural rubber (NR) has traditionally come from *Hevea brasiliensis* trees which are native to South America's Amazon forest and are commonly farmed in Southeast Asia today [9, 14]. Due to a variety of obstacles ranging from diseases, pests, climate impacts, and geopolitical considerations, the supply of *Hevea brasiliensis* rubber is vulnerable and so too are industries like tire manufacturing that use it as their primary source of NR. As a result, there has been increasing interest in other sources of NR like dandelion flower roots, guayule shrub bark, and *Eucommia ulmoides* trees to list a few. Currently, research into alternative sources of NR is in its early stages, investigating how to selectively breed, process, and remove impurities from the NR with the goal of future industrialization [9]. In contrast, synthetic rubbers have traditionally been synthesized from petrochemical byproducts and often exhibit inferior mechanical properties compared to NR [9, 15]. With shortages in petrochemical starting materials and the global push towards more sustainable materials, there has been research into additional synthetic rubbers made from bio-based monomers and other forms of biomass/biowaste. Some of these synthetic bio-based rubbers include varieties of itaconate and thermoplastic elastomers [9].

Tire cords can be thought of as the skeletal structure of the tire and have traditionally been made out of metals such as steel, synthetic textiles like nylon and polyester, or some combination of the two groups. Like with current synthetic rubbers, much of the synthetic textiles used are made from petrochemical sources, producing large amounts of pollution. Current research on more sustainable tire cords centers on materials such as lyocell fibers which are "a type of cellulose

fiber made by spinning cellulose pulp dissolved in a water solution of N-methylmorpholine-N-oxide (NMMO)” [9]. Additionally, recycled PET fibers are of interest since the base PET can be sourced from used PET bottles and from PET waste fabrics. Over 90% of recycled PET fibers are made of used PET bottles today. There has also been development of biobased polyamide fibers made from biomass like crop straw. Despite these advancements in more sustainable tire cord materials, these new materials are still in development, requiring refinement on various synthesis and processing techniques to produce less variable materials that meet the mechanical demands of tire cords [9].

In the realm of tire additives, the replacement of traditional filler materials such as carbon black is a crucial step in improving the environmental sustainability of tire materials. While recycled carbon black (via pyrolysis) is increasingly being used in the fabrication of new tires, current research indicates there is a limit to the percentage of recycled carbon black (compared to virgin carbon black) that can be used in new tires before wear resistance and overall performance of the tire begin to decrease. The utilization of agricultural waste to form new filler materials is often seen as a way to minimize environmental impacts. Biochars made from the burning of “low-ash nutshell feedstocks (hazelnut and walnut) and two high-silica grain husk feedstocks (oat and rice)” are two such examples [9]. For the case of the nutshell biochar specifically, researchers found using the biochar as a filler material resulted in rubber with reinforcement properties on par with or greater than that of carbon black rubbers, and the mechanical properties of the biochar rubber could be further improved through activation of the biochar in a slurry [9].

Similar research has been conducted into the use of silica as a more sustainable filler material in automobile tires. Traditionally, silica has not been widely used in the tire industry due to factors like high cost, issues with processing, and inferior chemical reactivity compared to carbon black.

Compared to precipitated silica, carbon black has more active surface sites which allows greater connectivity and compatibility with a larger variety of rubbers without needing surface modification treatments. Traditional silica is also hydrophobic and includes numerous highly polar functional groups, making it incompatible with nonpolar elastomers, preventing its even dispersion in the rubber matrix, and diminishing desired mechanical properties [16].

Given these issues, researchers have investigated alternative sources of silica like from plant material. The utilization of agricultural waste is advantageous in a variety of ways like low cost, decreased energy consumption, and easy availability. Agricultural waste sources include rice husks, corn stalks, sugar cane, and bamboo which are turned into ash to access the high percentages of silica within them. Compared to traditional silica, biobased silica is more reactive with silicone functional groups, resulting in better dispersion within the rubber matrix and improved mechanical properties [16]. Research into the use of rice husk ash as a filler material corroborated these findings. Researchers found the rice husk ash was able to better disperse in the rubber matrix and improve mechanical properties such as the tensile strength and elongation at break. Additional research has also investigated the extraction of other materials from renewable sources with potential as alternative filler materials like graphite, carbon nanotubes, cellulose, and lignin [9].

Of particular relevance to the scope of this research is the utilization of lignin as a renewable tire filler material. Lignin is a polymer found in plant biomass such as trees, stems/stalks, grasses, and paper industry and sawmill waste. There are three main types of natural lignin including softwood, hardwood, and grass lignin. There are also kinds of industrially modified lignin like soda glass and kraft lignin [17]. Lignin is one of three polymers found within plant biomass in addition to cellulose and hemicellulose, and the exact quantities of each polymer vary depending

on factors like the original plant source, its age, the season it was harvested, and other environmental conditions [18]. After cellulose, lignin is thought to be the second most plentiful renewable natural polymer found on Earth [17]. While the exact composition and structure of lignin varies depending on biomass source, lignin's 3D structure is generally made from the crosslinking of three different phenyl propane units or monolignols: para-coumaryl alcohol, coniferyl alcohol, and sinapyl alcohol. These base monolignols then group together to form lignin's base building blocks p-hydroxyphenyl (H), guaiacyl (G), and syringyl. Within plants, lignin intertwines with cellulose and hemicellulose to form lignocellulosic biomass which forms a "strong stretch network in the cell wall and recalcitrant biomass" [18]. Via covalent bonds and hydrogen bonds, lignin acts as the binding agent in cell walls, filling the remaining space between cellulose and hemicellulose [18, 19].

As a material, lignin is valued for its easy availability, low cost, biodegradability, antimicrobial behavior, and adhesive properties [18]. The paper industry and industrial agriculture produce large amounts of lignin every year through their waste, and the generated lignin can be easily separated out from the bulk biomass waste [18, 20]. Due to the presence of polar functional groups within lignin, lignin can effectively bond to numerous pollutants and heavy metals. This makes lignin-based materials ideal for applications in environmental pollution clean up where it can effectively adsorb these harmful materials [19]. Utilization of lignin in its original form is limited though due in part to its polarity. Within rubber composites, specifically, lignin often must undergo chemical modification before it can be effectively dispersed in the rubber matrix. Without chemical treatments, the lignin would aggregate together due to high self-adhesion caused by its polarity [20, 21]. Lignin also has a high glass transition temperature which makes the incorporation of higher percentages of lignin and melt processing difficult [20].

For applications in rubber composites, various chemical treatments for lignin have been developed to improve the dispersion of the lignin within the rubber matrix and increase the adhesion of lignin to rubber macromolecules [20, 21]. Some chemical treatments of lignin have included surface modification with poly (diallyldimethylammonium chloride), layered double hydroxide, montmorillonite, and cyclohexylamine [17]. Additional modification treatments have utilized a variety of organic solvents, numerous purification stages, acid treatments, polyelectrolytes, and the incorporation of other filler materials in addition to the lignin [20]. For example, tannic acid was combined with lignin and glyoxal (all biomass derivatives) to improve the adhesive nature of a solution that was used to adhere PI fibers to rubber. As a result of the treatment with tannic acid, the lignin-based adhesive improved in effectiveness, increasing the interfacial adhesion between the PI fibers and rubber [22]. The incorporation of lignin into rubber-based composites also has the potential to facilitate self-healing of the rubber matrix which would be particularly useful for rubber composites like those in automobile tires which experience high environmental and performance demands, but more research is needed to determine the specifics of this potential ability [23].

Despite these apparent advantages of lignin from increased environmental sustainability to improved mechanical and chemical characteristics in the final rubber composite, only 2% of lignin generated by the paper industry has been effectively utilized in industrial processes like the fabrication of new goods/materials. Instead, lignin is often burned as a low quality fuel [17]. In addition to aiming to fabricate renewable tire materials that have a lower environmental impact when compared to traditional tires, this research is in partnership with a tire material start-up, fitting into the broader context of innovation in automobile tires since the startup seeks to expand the feasibility and industrial use of waste lignin in composite rubbers.

MATERIALS AND METHODS

A. Sample Formulation

Prior to the mixing of individual samples, a stock formulation of centrifuged natural rubber (NR) latex (61% solids) and DP50201 lignin solution (49% solids) was first created. The lignin solution (sourced from LignoTech) was first measured at a starting mass of 54.034 g. Next, 100.870 g of the NR latex solution was weighted into a narrow diameter vessel. The NR latex solution was then placed beneath a viscometer which was then set at 700 RPM until a mild vortex was achieved. The lignin solution was then slowly streamed into the NR latex vortex until a homogenous mixture was achieved. The resulting stock formulation had roughly 57% solids. A portion of the NR-lignin stock formulation was then diluted further using DI water until a solution with roughly 0.11% solids was achieved.

The 0.11% solids solution was then used directly to create all individual samples. All samples consisted of 1.2 mL of the 0.11% solids solution plus 0.3 mL of additional additives. The control group sample included an additional 0.3 mL of DI water. Acidic conditions samples were created by combining the base 1.2 mL of the 0.11% solids solution with varying amounts of a HCl stock solution and DI water to achieve samples with 25, 50, 75, and 100 mM final concentrations of HCl. Similarly, the basic and ionic conditions samples were created by combining the base 1.2 mL of the 0.11% solids solution with varying amounts of a NaOH/NaCl stock solution and DI water to achieve samples with 25, 50, 75, and 100 mM final concentrations of NaOH/NaCl. The resulting final volume of all individual samples was approximately 1.5 mL. Besides the control group sample, all sample conditions groups (*i.e.*, acidic, basic, and ionic) included four individual samples, resulting in 13 total samples.

B. Dynamic Light Scattering Testing

After mixing each individual sample in their own small cylindrical glass cuvette, each sample was evaluated using dynamic light scattering (DLS) at a constant temperature of 22°C. An LS Spectrometer II (produced by LS Instruments) was used to conduct all DLS testing. All samples were tested with the following protocol: loop angular sweeps from 150° to 30° with steps of 15° (*i.e.*, nine angles measured for each sample), target scattering intensity of 200.0 *kHz*, five measurements at each angle (each for 30 seconds). The full protocol took roughly 30 minutes to complete for each sample. All collected data files for each sample were then exported and analyzed via MATLAB. All provided figures were also created using MATLAB.

RESULTS AND DISCUSSION

A. Autocorrelation Function

After completing DLS testing for all 13 samples, the resulting raw data was processed via MATLAB. For a single sample, all five repetitions at a single angle were averaged, and then the standard error was calculated for each averaged data point. Standard error S.E. was calculated using equation A.1 where the mean value μ is an individual averaged data point, σ is the standard deviation of a single measurement, and n is the total number of initial values that had been averaged (*i.e.*, five repetitions in the case of all presented experiments within this report):

$$S. E. = \frac{\sigma(\mu)}{\sqrt{n}} \quad (\text{A.1})$$

The processed autocorrelation function data at all tested angles for the control group sample is presented in Figure 1. The solid-colored plotted line represents the averaged $g_2 - 1$ data, and the standard error between those averaged values is depicted as a matching-color shaded region around the averaged $g_2 - 1$ line.

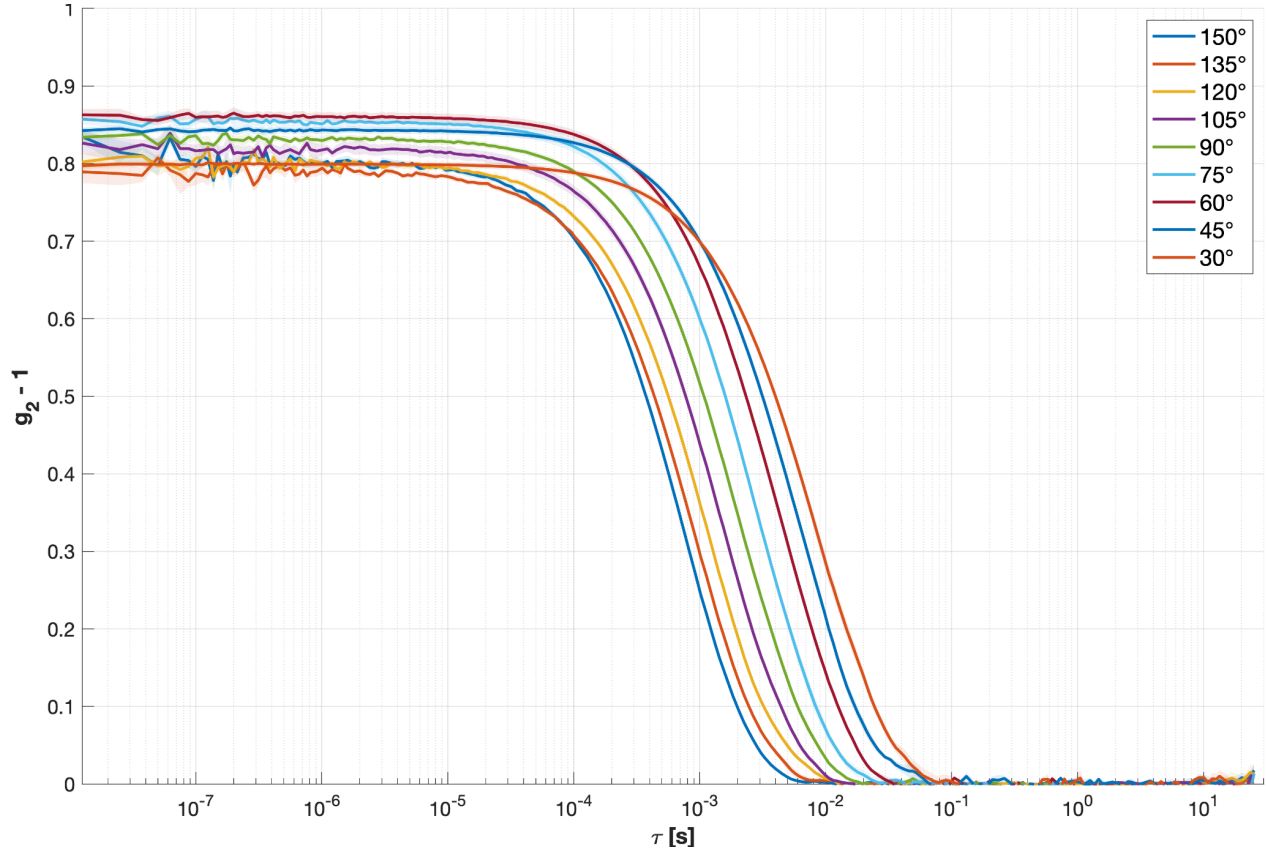


Figure 1: Plot of the resulting autocorrelation function $g_2 - 1$ as a function of lag time τ for the control group sample at all nine evaluated angles. Data collected via DLS.

As depicted in Figure 1, the autocorrelation function is close to its maximum value (somewhere between 0.8 and 0.9) at low lag times, indicating the received light signal from one time point to the next are close in value to each other. This means the particles in the solution that are scattering the emitted light are not moving much from their original positions at these short observation times. As the observation time increases though, the particles undergo Brownian motion, moving randomly away from their starting positions and decreasing the value of $g_2 - 1$ [24]. A steeper decay in the autocorrelation function indicates a faster diffusion rate of particles (*i.e.*, smaller particles), and the opposite relationship is true for a shallower decay of the autocorrelation function [25]. In Figure 1, large observation angles such as 150° result in the

study of comparatively smaller particles than lower observation angles such as 30° since the slope of $g_2 - 1$ at 150° decays faster than the corresponding 30° $g_2 - 1$ line. The change in observed autocorrelation at different angles is a result of the change in scattering wave vector; measurements at higher angle are probing larger wave vectors or smaller distances while measurements at small angle correspond to small wave vectors or larger distances. The variable-angle DLS results then provide another metric for the distribution in size and shape. Such a shift in the $g_2 - 1$ curve with varying observation angle is as to be expected for large, polydisperse samples such as the NR latex–lignin solution evaluated throughout this study.

To allow better comparison of sample condition groups to each other and the control group sample, the averaged autocorrelation function data for all samples in a condition group were plotted versus the control group sample 90° . 90° was chosen to correspond to the highest scattering intensity and a standard choice in light scattering measurements. More complex analysis of the Mie scattering patterns will permit future deconvolution of the distribution by analyzing all scattering angles. All acidic conditions samples versus the control sample at 90° are depicted in Figure 2. All basic conditions samples versus the control sample at 90° are depicted in Figure 3. All ionic conditions samples versus the control sample at 90° are depicted in Figure 4.

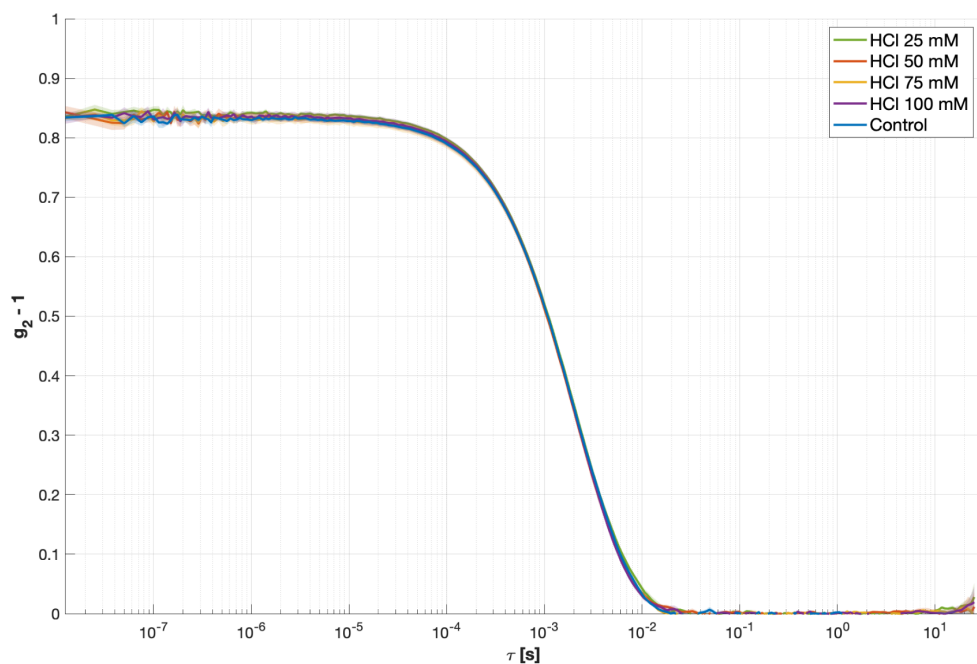


Figure 2: Comparison of the resulting autocorrelation function $g_2 - 1$ as a function of lag time τ for the control group sample versus all acidic conditions samples at 90° .

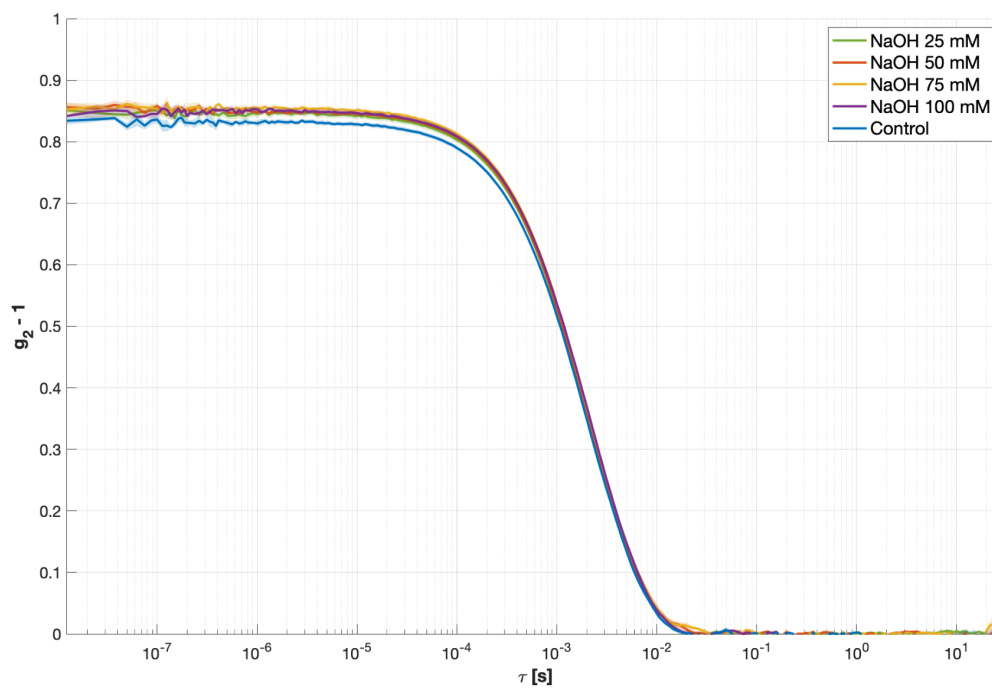


Figure 3: Comparison of the resulting autocorrelation function $g_2 - 1$ as a function of lag time τ for the control group sample versus all basic conditions samples at 90° .

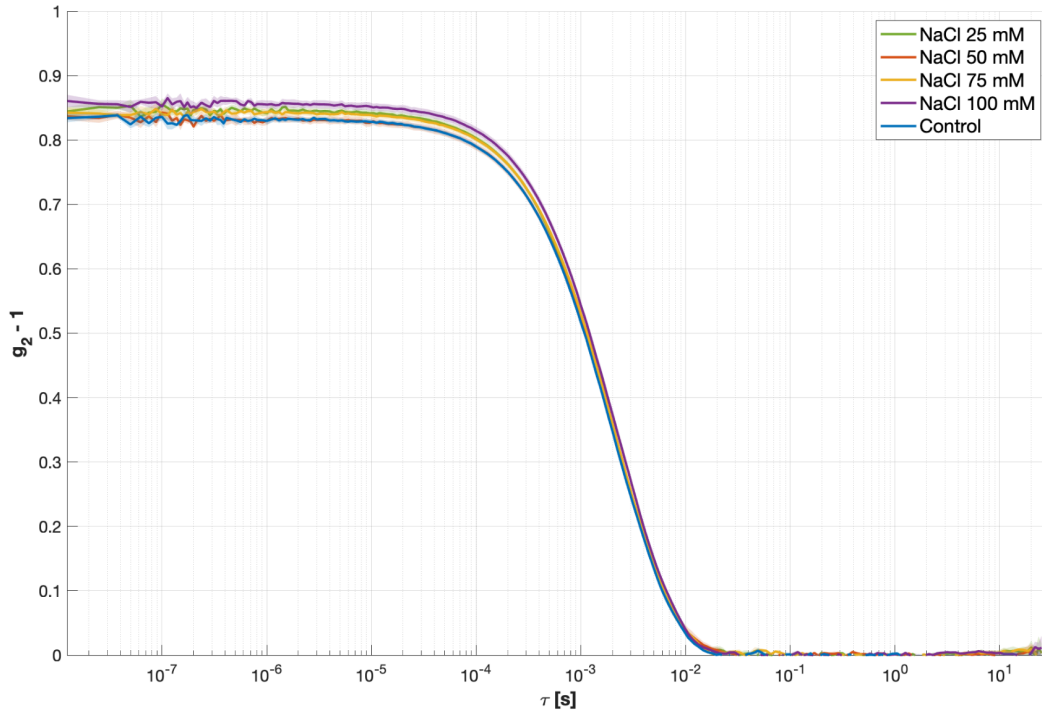


Figure 4: Comparison of the resulting autocorrelation function $g_2 - 1$ as a function of lag time τ for the control group sample versus all ionic conditions samples at 90° .

As depicted in Figure 2 and Figure 3, the impact of acidic and basic conditions on the NR latex–lignin solution has minor impacts on the shape of the $g_2 - 1$ curves. The maximum $g_2 - 1$ values for the basic conditions samples are slightly higher than that of the control group sample. As a result of the shift in the $g_2 - 1$ curve upward, the decay rate is slightly higher for the basic conditions samples than the control group sample, indicating a slightly slower particle diffusion rate (*i.e.*, larger observed particles) at 90° . Similarly, ionic conditions (depicted in Figure 4) also had a limited impact on the shape and subsequent decay rate of the plotted $g_2 - 1$ curve. Like the basic conditions samples, the ionic conditions samples had slightly raised maximum $g_2 - 1$ values compared to the control group sample and corresponding higher decay

rate, indicating a slightly slower particle diffusion rate (*i.e.*, larger observed particles) at 90° compared to that of the control group sample.

B. CORENN Intensity

CORENN relative intensity data is derived by using the CORENN fitting algorithm (native to the LS Spectrometer II desktop software) to invert the autocorrelation function $g_2 - 1$, transforming the collected data into a plot of the relative distribution or intensity of different sized particles within the sample. This additional method of representing collected data is important as it allows insight into the relative sizes of particles in a sample, the rough distribution/prevalence of different sized particles, and overall polydispersity of the sample.

Like what was done to the raw autocorrelation function data, the individual CORENN intensity data for a single sample was averaged across all five repetitions, and then the standard error was calculated for each averaged data point, also using equation A.1. The processed CORENN intensity data as a function of *hydrodynamic radius* at all tested angles for the control group sample is presented in Figure 5. The solid-colored plotted line represents the averaged *relative intensity* data, and the standard error between those averaged values is depicted as a matching-color shaded region around the averaged *relative intensity* line. Note: averaging the CORENN intensity distributions obtained from individual autocorrelation functions was done rather than doing a CORENN analysis of the averaged autocorrelation functions. While the chosen method leads to significantly more noise, it provides insight into the ergodicity of the sample and avoids an overly broad distribution by pre-averaging.

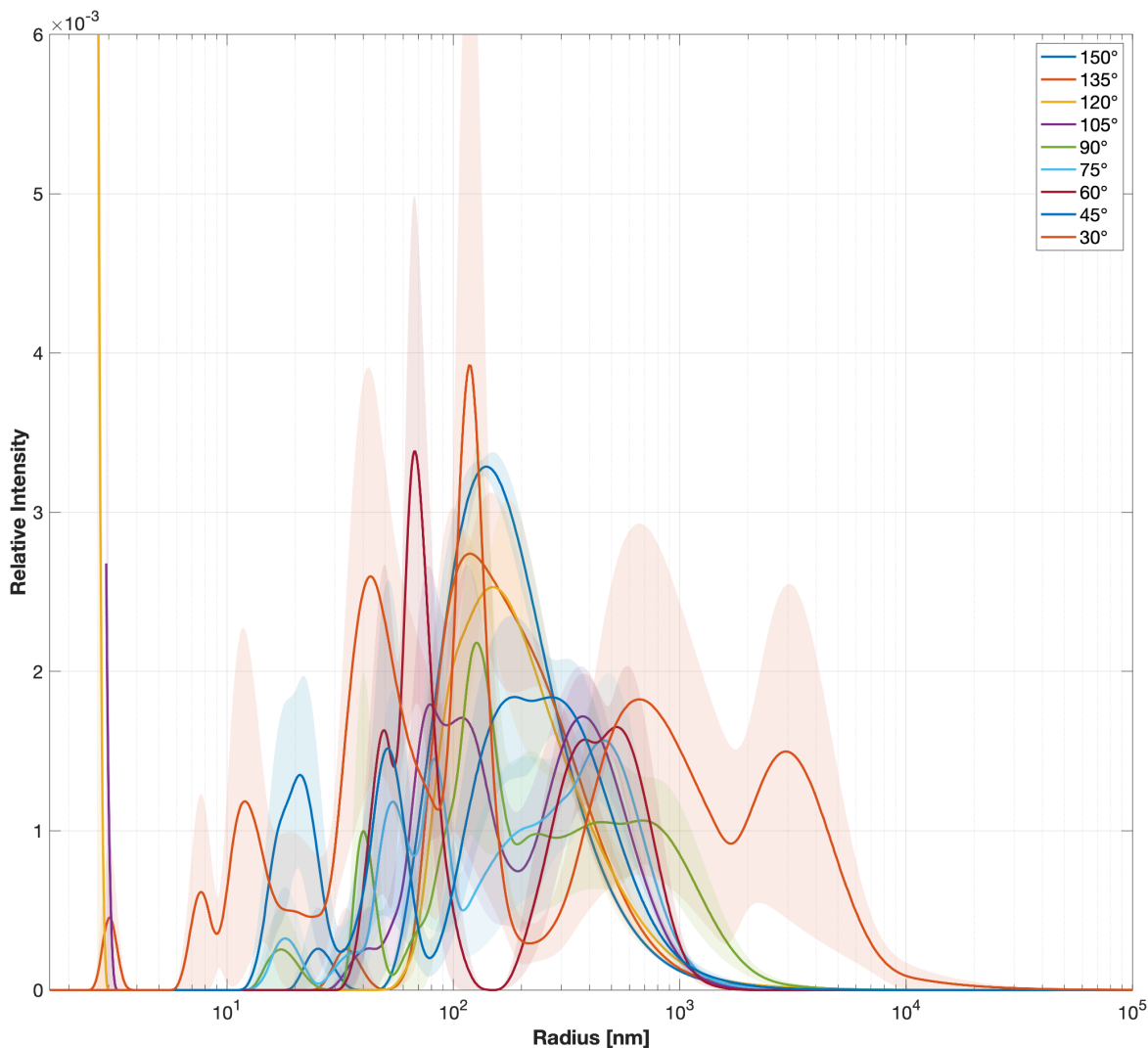


Figure 5: Plot of the resulting CORENN intensity data as a function of hydrodynamic radius for the control group sample at all nine evaluated angles. Data collected via DLS.

As depicted in Figure 5, the control group NR latex and lignin sample was fairly polydisperse, having a wide range of detected particle sizes across the nine different angles tested. Particles had hydrodynamic radii values primarily in the range of ~ 10 nm to $\sim 10^4$ nm with the highest number of measured particles having sizes of roughly 10^2 nm.

To allow better comparison of sample condition groups to each other and the control group sample, the averaged CORENN intensity data for all samples in a condition group were plotted

versus the control group sample 90° . All acidic conditions samples versus the control sample at 90° are depicted in Figure 6. All basic conditions samples versus the control sample at 90° are depicted in Figure 7. All ionic conditions samples versus the control sample at 90° are depicted in Figure 8.

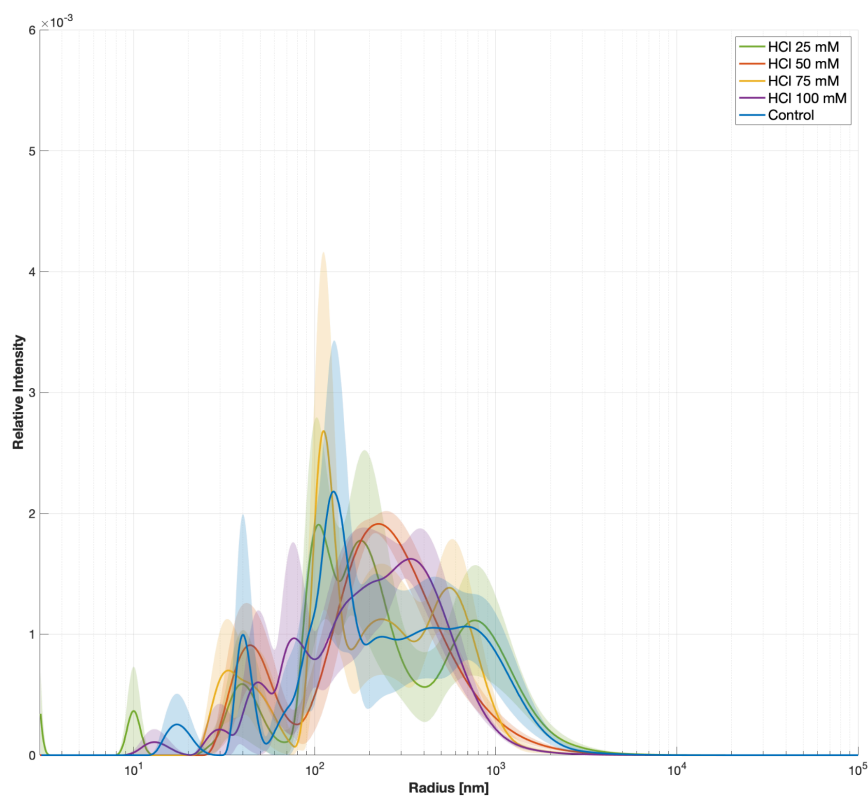


Figure 6: Comparison of the resulting CORENN intensity data as a function of hydrodynamic radius for the control group sample versus all acidic conditions samples at 90° .

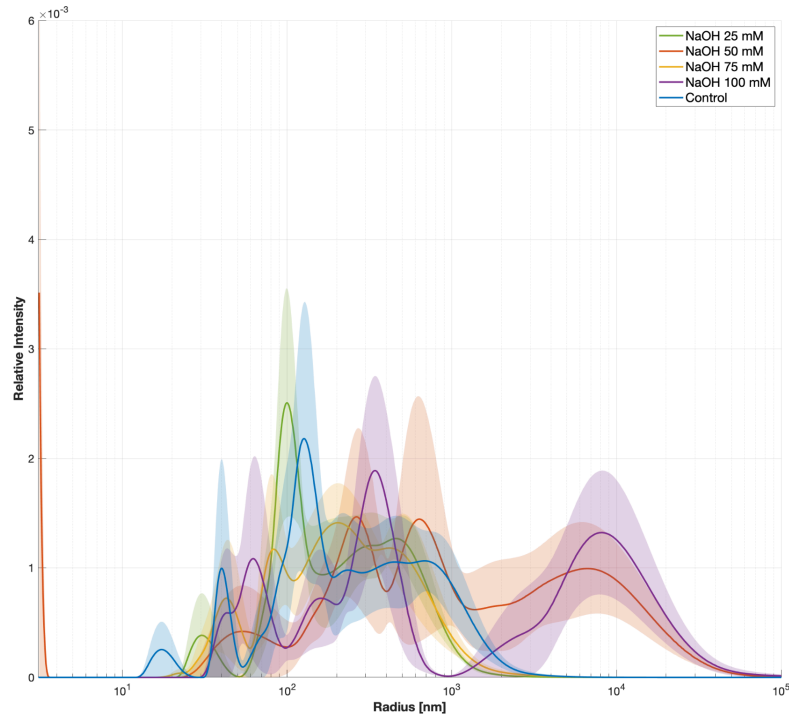


Figure 7: Comparison of the resulting CORENN intensity data as a function of hydrodynamic radius for the control group sample versus all basic conditions samples at 90° .

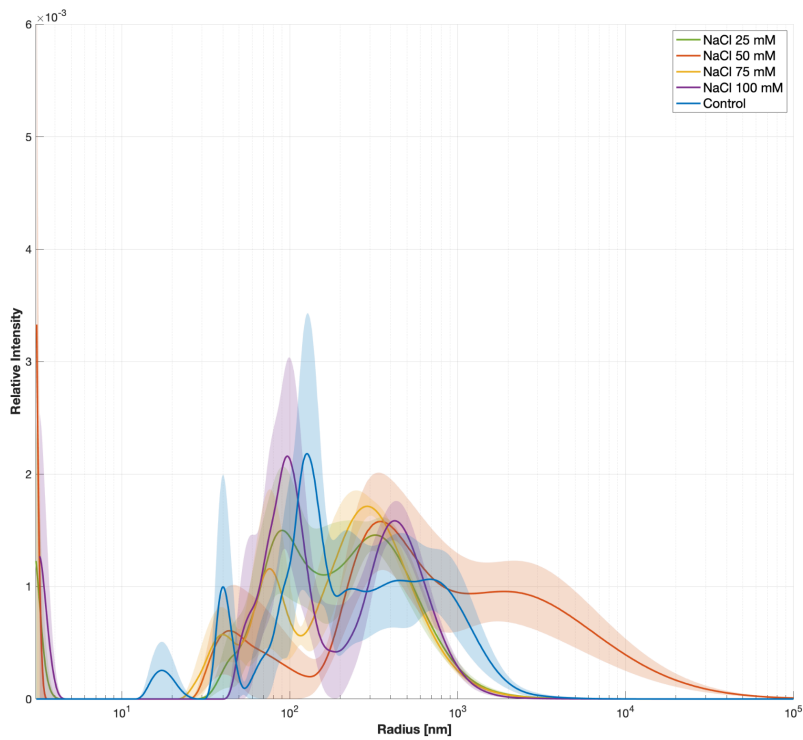


Figure 8: Comparison of the resulting CORENN intensity data as a function of hydrodynamic radius for the control group sample versus all ionic conditions samples at 90° .

As depicted in Figure 6, the application of acidic conditions on the NR latex and lignin solution appears to slightly stabilize it, resulting in a slightly smaller distribution of particle sizes when compared to the control group. In addition, the shaded standard error regions appear thinner for the acidic group samples (especially the 50 *mM* sample) compared to the control group sample, indicating less variation in the actual relative intensity/distribution measurements of particulates at a given hydrodynamic radius size.

In contrast, the application of basic conditions to the NR latex–lignin solution has the opposite effect, as seen in Figure 7. Instead of reducing the distribution of particle sizes like in the acidic conditions samples, the basic conditions samples have a wider range of measured hydrodynamic radii, with new relative intensity peaks for particulates of $\sim 10^4$ *nm*. In addition to the wider distribution of measured particle sizes in the basic conditions group, the standard error regions were roughly the same if not larger (in the case of the 50 *mM* and 100 *mM* samples) than the plotted control group sample's standard error. Similarly, the application of ionic conditions (as seen in Figure 8) to the NR latex–lignin solution resulted in a wider distribution of particle sizes although not as extreme as when basic conditions were applied. In both the basic conditions and ionic conditions samples, there also appears to be a greater number of particles smaller than 10 *nm* in size than the acidic conditions samples, but this is likely an artifact related to cross-correlation effects at very short lag times.

C. Impact of Additives on Hydrodynamic Radius

Like what was done to the raw correlation function and CORENN intensity data, the mean hydrodynamic radius for each of the five repetitions for a single sample was averaged, and then the standard error was calculated for each sample, also using equation A.1. The processed mean

hydrodynamic radius values as a function of concentration of additives (*i.e.*, HCl, NaOH, or NaCl) for all samples at 90° is presented in Figure 9. The standard error of each sample's mean hydrodynamic radius is depicted as an error bar, centered on the corresponding data point. To improve readability of the figure, all sample conditions groups were plotted in the same color.

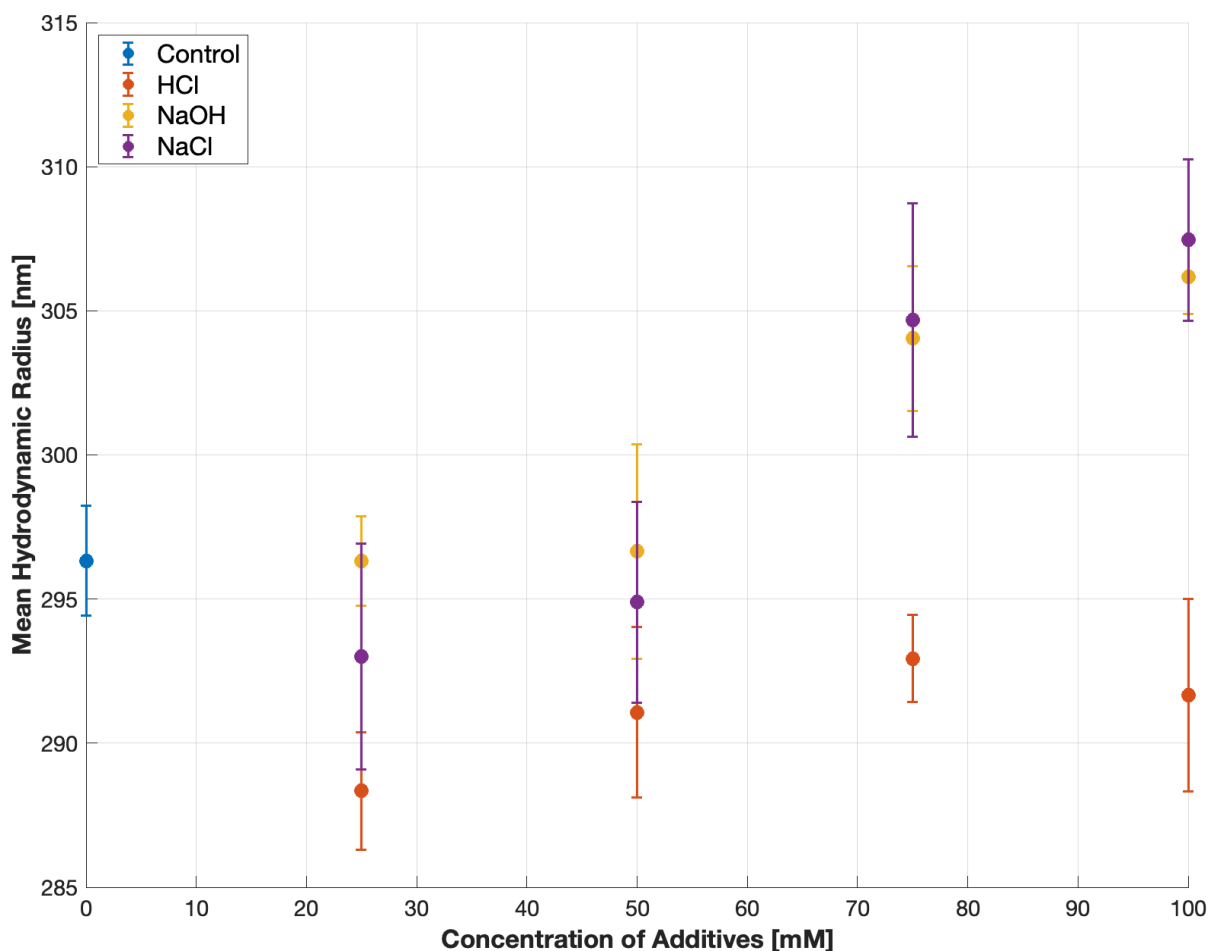


*Figure 9: Comparison of mean hydrodynamic radius as a function of concentration of additives (*i.e.*, HCl, NaOH, or NaCl) in the tested sample at 90°. All 13 tested samples are depicted in this plot with color coating corresponding to the sample conditions group.*

Figure 9 helps to support earlier findings that the application of acidic conditions helps to stabilize the NR latex–lignin solution. As depicted in Figure 6, the application of acidic conditions helped to slightly reduce the size distribution of particles in the solution and also

reduce the measured standard error. The acidic samples in Figure 9 had smaller mean hydrodynamic radius values than the control group sample and had relatively small standard error regions (especially for the 25 *mM* and 75 *mM* samples).

In contrast, the basic and ionic conditions samples had roughly the same or slightly larger/smaller mean hydrodynamic radius values than the control group sample at additive concentrations at or lower than 50 *mM*. In the case of NaOH or NaCl concentrations greater than 50 *mM*, the mean hydrodynamic radius values for both condition groups are considerably larger than that of the control group sample. In addition, the ionic conditions samples had a consistently large standard error range compared to the acidic and basic conditions samples which appeared to experience variation in the standard error value between samples at different measured concentrations of additives.

Regarding limitations of the data presented in Figure 9 specifically, the plotted mean hydrodynamic radius values (and their respective standard error values) were determined by taking the provided mean hydrodynamic radius at each of the five repetitions for a single sample at 90° and averaging those. The standard error was determined by taking the standard deviation of those already average values (for an individual run) and dividing the square root of the total number of runs at a single angle (*i.e.*, five repetitions). This calculation does not account for the true variability in hydrodynamic radius between all conducted repetitions at a given sample, so the standard error for each sample should especially be treated with caution. Ideally, a more thorough analysis of the true mean hydrodynamic radius (and its variability) at a given angle could be conducted, but due to limited time, that kind of analysis was not feasible for this report.

FUTURE WORK

Based on initial findings in this report regarding the (slightly) stabilizing impact of acidic conditions on the tested NR latex–lignin solution, more thorough experimentation such as examining the impact of other acids, evaluating behavior at a greater range of concentrations, and testing resulting solution pH could all be potential areas of future research. In addition, the NR latex–lignin solution tested in this study only consisted of the base NR latex and lignin solutions that were purchased, not including any other potential chemical additives such as Hexamethylenetetramine (HMT) and Carboxyl-Methyl-Cellulose (CMC) which are currently used in the partnered tire-material startup’s rubber formulation. Additional testing with these two additives could all be potential areas of future research. Given the partnered tire-material startup’s eventual goal of being able to 3D print the uncured rubber formulation, additional future testing on the impact of these additives (including any acids added to help stabilize the initial NR latex–lignin matrix) on viscosity (in addition to extent of phase separation over time) is needed to make this goal a reality. Rheological cure studies would also be beneficial in determining how the flow behavior of the uncured rubber solution changes as it is vulcanized and how that behavior varies with different additives/quantities of additives.

REFERENCES

- [1] International Energy Agency (IEA), “World Energy Outlook 2022,” *IEA*, Oct. 2022, Available:
<https://iea.blob.core.windows.net/assets/830fe099-5530-48f2-a7c1-11f35d510983/WorldEnergyOutlook2022.pdf>
- [2] A. Mohajerani *et al.*, “Recycling waste rubber tyres in construction materials and associated environmental considerations: A review,” *Resources, Conservation and Recycling*, vol. 155, p. 104679, Apr. 2020, doi:
<https://doi.org/10.1016/j.resconrec.2020.104679>.
- [3] V. Bijina, P. J. Jandas, S. Joseph, J. Gopu, K. Abhitha, and H. John, “Recent trends in industrial and academic developments of green tyre technology,” *Polymer Bulletin*, 2023, doi: <https://doi.org/10.1007/s00289-022-04445-2>.
- [4] M. Kida, S. Ziembowicz, Kamil Pochwat, and Piotr Koszelnik, “Experimental and computational hazard prediction associated with reuse of recycled car tire material,” vol. 438, pp. 129489–129489, Jun. 2022, doi: <https://doi.org/10.1016/j.jhazmat.2022.129489>.
- [5] M. S. Mashiri, J. S. Vinod, M. N. Sheikh, and H.-H. Tsang, “Shear strength and dilatancy behaviour of sand–tyre chip mixtures,” *Soils and Foundations*, vol. 55, no. 3, pp. 517–528, Jun. 2015, doi: <https://doi.org/10.1016/j.sandf.2015.04.004>.
- [6] Z. Xiao, A. Pramanik, A. K. Basak, C. Prakash, and S. Shankar, “Material recovery and recycling of waste tyres-A review,” *Cleaner Materials*, vol. 5, p. 100115, Jul. 2022, doi: <https://doi.org/10.1016/j.clema.2022.100115>.

- [7] E. S. Rødland, G. Binda, Davide Spanu, Stefano Carnati, Laura Röhler Bjerke, and Luca Nizzetto, “Are eco-friendly ‘green’ tires also chemically green? Comparing metals, rubbers and selected organic compounds in green and conventional tires,” *Journal of Hazardous Materials*, vol. 476, pp. 135042–135042, Sep. 2024, doi: <https://doi.org/10.1016/j.jhazmat.2024.135042>.
- [8] T.-H. Lin, Y.-S. Chien, and W.-M. Chiu, “Rubber tire life cycle assessment and the effect of reducing carbon footprint by replacing carbon black with graphene,” *International Journal of Green Energy*, vol. 14, no. 1, pp. 97–104, Nov. 2016, doi: <https://doi.org/10.1080/15435075.2016.1253575>.
- [9] S. Deng, R. Chen, S. Duan, Q. Jia, X. Hao, and L. Zhang, “Research progress on sustainability of key tire materials,” *SusMat*, vol. 3, no. 5, pp. 581–608, Sep. 2023, doi: <https://doi.org/10.1002/sus2.159>.
- [10] M. A. González, María Altagracia Rodríguez-Sosa, Yohan Enmanuel Vásquez-Bautista, Elizabeth, Jesús Confesor Durán-Tiburcio, and Doddy Prayogo, “A survey of tire-breeding mosquitoes (Diptera: Culicidae) in the Dominican Republic: Considerations about a pressing issue,” vol. 40, no. 3, pp. 507–515, Sep. 2020, doi: <https://doi.org/10.7705/biomedica.5200>.
- [11] I. Čabalová, A. Ház, J. Krilek, T. Bubeníková, J. Melicherčík, and T. Kuvik, “Recycling of Wastes Plastics and Tires from Automotive Industry,” *Polymers*, vol. 13, no. 13, p. 2210, Jul. 2021, doi: <https://doi.org/10.3390/polym13132210>.
- [12] A. Hamdi, G. Abdelaziz, and K. Z. Farhan, “Scope of reusing waste shredded tires in concrete and cementitious composite materials: A review,” *Journal of Building*

- Engineering*, vol. 35, p. 102014, Mar. 2021, doi: <https://doi.org/10.1016/j.jobe.2020.102014>.
- [13] A. Shahi, C. Dwivedi, and S. Manjare, “Experimental and theoretical investigation on pyrolysis of various sections of the waste tire and its components,” *Chemical Engineering Research and Design*, vol. 179, pp. 66–76, Mar. 2022, doi: <https://doi.org/10.1016/j.cherd.2021.12.022>.
- [14] J. Thomas and R. Patil, “The Road to Sustainable Tire Materials: Current State-of-the-Art and Future Perspectives,” *Environmental Science & Technology*, vol. 57, no. 6, pp. 2209–2216, Feb. 2023, doi: <https://doi.org/10.1021/acs.est.2c07642>.
- [15] S. Kawahara, H. Nishioka, M. Yamano, and Y. Yamamoto, “Synthetic Rubber with the Tensile Strength of Natural Rubber,” *ACS Applied Polymer Materials*, vol. 4, no. 4, pp. 2323–2328, Mar. 2022, doi: <https://doi.org/10.1021/acsapm.1c01508>.
- [16] B. Shoul, Y. Marfavi, B. Sadeghi, E. Kowsari, P. Sadeghi, and S. Ramakrishna, “Investigating the potential of sustainable use of green silica in the green tire industry: a review,” *Environmental Science and Pollution Research*, vol. 29, no. 34, pp. 51298–51317, May 2022, doi: <https://doi.org/10.1007/s11356-022-20894-8>.
- [17] K. Roy, S. C. Debnath, and P. Potiyaraj, “A Review on Recent Trends and Future Prospects of Lignin Based Green Rubber Composites,” *Journal of Polymers and the Environment*, vol. 28, no. 2, pp. 367–387, Dec. 2019, doi: <https://doi.org/10.1007/s10924-019-01626-5>.

- [18] M. Eqbalpour, Amirhossein Andooz, Elaheh Kowsari, S. Ramakrishna, Zahra Ansari Cheshmeh, and Amutha Chinnappan, “A comprehensive review on how ionic liquids enhance the pyrolysis of cellulose, lignin, and lignocellulose toward a circular economy,” *Wiley interdisciplinary reviews. Energy and environment*, vol. 12, no. 4, Mar. 2023, doi: <https://doi.org/10.1002/wene.473>.
- [19] P. G, S. AS, J. S. Jayan, A. Raman, and A. Saritha, “Lignin based nano-composites: Synthesis and applications,” *Process Safety and Environmental Protection*, vol. 145, pp. 395–410, Jan. 2021, doi: <https://doi.org/10.1016/j.psep.2020.11.017>.
- [20] S. Hait *et al.*, “Unlocking the Potential of Lignin: Towards a Sustainable Solution for Tire Rubber Compound Reinforcement,” *Journal of Cleaner Production*, pp. 143274–143274, Jul. 2024, doi: <https://doi.org/10.1016/j.jclepro.2024.143274>.
- [21] Federica Ferruti *et al.*, “Mechanochemical Methacrylation of Lignin for Biobased Reinforcing Filler in Rubber Compounds,” *ACS Sustainable Chemistry & Engineering*, Sep. 2024, doi: <https://doi.org/10.1021/acssuschemeng.4c05036>.
- [22] H. Li *et al.*, “Lignin Biobased Eco-Friendly Dipping System for Polyimide Fiber and Its Interface Adhesive Mechanism with Rubber,” *Industrial & Engineering Chemistry Research*, Jun. 2024, doi: <https://doi.org/10.1021/acs.iecr.4c01129>.
- [23] Bedriye Nur Yeşil, Tuba Ünügül, and Bağdagül Karaağaç, “Self-healing behaviour of lignin-containing epoxidized natural rubber compounds,” *Express Polymer Letters*, vol. 17, no. 7, pp. 704–721, Jan. 2023, doi: <https://doi.org/10.3144/expresspolymlett.2023.53>.

- [24] W. Basel, “LS Instruments | Theory,” *Lsinstruments.ch*, 2024. <https://lsinstruments.ch/en/theory/dynamic-light-scattering-dls/theory> (accessed Apr. 23, 2025).
- [25] R. J. Young and P. A. Lovell, *Introduction to Polymers*, 3rd ed. Boca Raton: Crc Press, 2011.